Terahertz magneto-optical properties of Nitrogen-doped diamond

Terahertz optoelectronic properties of synthetic single crystalline diamond

Huan Xiao [a,1], Zongyan Zhang [b,1], Wen Xu [c,a,d,], Qiujing Wang [a], Yiming Xiao [a,**], Lan Ding [a], Jiangtao Huang [b], Haowen Li [c], Bin He [b,***], Francois M. Peeters [c,e,f]*

[a] School of Physics and Astronomy and Yunnan Key laboratory of Quantum Information, Yunnan University, Kunming 650091, China

[b] College of New Materials and New Energies, Shenzhen Technology University, Shenzhen 515118, China

[c] Micro Optical Instruments Inc., Shenzhen 518118, China

[d] Key Laboratory of Materials Physics, Institute of Solid State Physics, HFIPS, Chinese Academy of Sciences, Hefei 230031, China

[e] Department of Physics, University of Antwerp, Groenenborgerlaan 171, B-2020 Antwerpen, Belgium

[f] Universidade Federal do Ceará, Departamento de Física, Caixa Postal 6030, 60455-760 Fortaleza, Ceará, Brazil

Highlights (85 words)

- Functional groups attached to the surface of synthetic single crystalline diamond (SCD) can result in terahertz (THz) optoelectronic responses.
- SCD does not show typical semiconductor characteristics in THz regime. A metallic to semiconductor transition can be observed at about 10 K via examining the temperature dependence of the electron density. There is a significant effect of photon-induced electronic backscattering in SCD.
- THz time-domain spectroscopy can be applied for measuring the transmittance, optical conductivity and dielectric constant of SCD with high dc resistivity.

* Corresponding author. Key Laboratory of Materials Physics, Institute of Solid State Physics, HFIPS, Chinese Academy of Sciences, Hefei 230031, China

** Corresponding author. School of Physics and Astronomy, Yunnan University, Kunming 650091, China.

*** Corresponding author. College of New Materials and New Energies, Shenzhen Technology University, Shenzhen 515118, China.

E-mail addresses: wenxu_issp@aliyun.com (W. Xu), yiming.xiao@ynu.edu.cn (Y.M. Xiao), hebin@sztu.edu.cn (B. He)

[1] Both authors make contributions to this work.

Terahertz optoelectronic properties of synthetic single crystalline diamond

Huan Xiao [a,1], Zongyan Zhang [b,1], Wen Xu [c,a,d,], Qiujing Wang [a], Yiming Xiao [a,**], Lan Ding [a], Jiangtao Huang [b], Haowen Li [c], Bin He [b,***], Francois M. Peeters [c,e,f]*

[a] School of Physics and Astronomy and Yunnan Key laboratory of Quantum Information, Yunnan University, Kunming 650091, China

[b] College of New Materials and New Energies, Shenzhen Technology University, Shenzhen 515118, China

[c] Micro Optical Instruments Inc., Shenzhen 518118, China

[d] Key Laboratory of Materials Physics, Institute of Solid State Physics, HFIPS, Chinese Academy of Sciences, Hefei 230031, China

[e] Department of Physics, University of Antwerp, Groenenborgerlaan 171, B-2020 Antwerpen, Belgium

[f] Universidade Federal do Ceará, Departamento de Física, Caixa Postal 6030, 60455-760 Fortaleza, Ceará, Brazil

Abstract

A systematic investigation is performed for the optoelectronic properties of single crystalline diamond (SCD) grown by microwave plasma chemical vapor deposition (MPCVD). It is indicated that, without any intentional doping during the sample growth, the terahertz (THz) optical conduction in SCD is mainly affected by H-terminations, -OH-, O- and N-based functional groups attached to the surface of SCD. By using THz time-domain spectroscopy (TDS), we have measured the transmittance, complex optical conductivity $\sigma(\omega)$ and dielectric constant of SCD. We find that SCD does not show typical semiconductor characteristics in THz regime, where $\sigma(\omega)$ cannot be described rightly by the conventional Drude formula. Via fitting the real part and imaginary parts of $\sigma(\omega)$ with the Drude-Smith formula, the electron density n_e, electronic relaxation time τ and electronic backscattering or localization factor have been determined optically. The temperature dependence of these parameters is also

measured. From the temperature dependence of n_e, a metallic to semiconductor transition is observed at about T=10 K. The temperature dependence of τ is mainly induced by electron coupling with acoustic-phonons and there is a significant effect of photon-induced electron backscattering or localization in SCD. This work demonstrates that THz TDS is a powerful technique in studying SCD which contains H- and O-based bonds and has low electron density and high dc resistivity. The interesting and important findings from this study can help us to gain an in-depth understanding of SCD and may provide new guidance for the applications of SCDs as electronic, optical and optoelectronic materials.

1. Introduction

The mechanical, thermal, electrical and optical properties of synthetic single crystalline diamonds (SCDs) are very close to these of natural diamonds [1-3]. The SCD has been already applied as an important and practical material in the fields of optics, electronics and optoelectronics [2]. For example, i) diamond is an excellent material for optical windows covering from X-ray and UV to terahertz (THz) under low-temperature and high-pressure conditions [3]; ii) it has unique quantum properties and is capable of optical and electrical control of nitrogen vacancy color centers at room temperature [4]. This was applied for high-precision magnetic field measurement [5], biological imaging [6], quantum detection [4], etc.; iii) SCD has been used as packaging material for semiconductor chips for extremely high thermal conductivity [7]; iv) due to its low atomic number, it has a large neutron scattering cross section and can be used in neutron detection [8]; v) it is an ultra-wide bandgap semiconductor which is important for application in the area of high power and high temperature electronics and integrated circuit chips [6, 9]. For the application of SCD in optical and electronic materials and devices, it is of great significance and importance to know the basic physical effects and parameters (especially optical and electrical effects and parameters) of diamonds. Electrical transport measurement has been commonly used for the characterization and investigation of SCD [10]. However, since SCD normally has high dc resistivity and low carrier density, the transport properties cannot be measured by

Hall effect method which requires the fabrication of ohmic contact electrodes [11]. As a result, the accuracy and signal-to-noise ratio of these electrical measurements on SCD are difficult to be controlled technically.

On the other hand, optical measurements [12] such as photoluminescence (PL) [13-14], Raman spectroscopy [15], UV-Vis absorption spectrum [16], FTIR spectrum [17], etc., are fast, easy, non-contacting and non-damaging techniques which has been applied for studying and characterizing of SCD. In recent years, the terahertz (THz) optoelectronic technique such as THz time-domain spectroscopy (TDS) [18] has been applied for the investigation of SCD. Because the THz photon energy (1 THz =4.13 meV) is much smaller than the bandgap of diamond, THz radiation can be utilized for the detection of free-carrier dynamics in SCD. In 2020, Amoruso et al. reported [19] the THz transmittance of diamond films in the presence of ultrafast laser irradiation. By using THz TDS, Ye et al. demonstrated [20] the fingerprint absorption peaks and complex dielectric response trends in 0.1-3.0 THz bandwidth in polycrystalline and monocrystalline diamond films grown by chemical vapor deposition (CVD). In 2021, Pang et al. applied femtosecond (fs) lasers to induce phase transformation in normal grade single crystal diamond flakes and showed that the optical and electrical properties of the radiated region were closely related to the degree of phase transformation [21]. These results indicate that THz techniques are powerful tools in the study of diamonds.

In comparison to Fourier spectroscopy, a major advantage of THz TDS technique is that it can obtain the complex optical coefficients (e.g., refractive index, dielectric constant, optical conductivity) of a sample in the frequency-domain without the help of the Kramers-Kronig (K-K) transformation of the experimental data. Thus, one does not need to use empirical or semi-empirical formulas for the K-K transformation in dealing with experimental data. Therefore, the real and imaginary parts of the complex optical coefficients can be obtained directly and more accurately via transmission or reflection measurements. To our knowledge, up to now there has been almost no research on the basic optoelectronic properties of SCD using THz TDS. This study aims to apply THz TDS to study and to measure accurately the basic optical coefficients of SCD with high dc resistivity and low electron density. We intend to determine the key electronic

parameters of SCD optically and to gain an in-depth understanding of SCD from the viewpoint of condensed matter physics and material applications.

2. Preparation and characterization of SCD

In this study, the microwave plasma chemical vapor deposition (MPCVD) (PLASSYS, SSDR150, France) was applied to grow single crystal diamond [15, 22], where pure hydrogen (H_2) 5 N and methane (CH_4) 5 N were used as the precursor gases. The plasma conditions were optimized by adjusting the input microwave power and the pressure in the chamber. During the growth of SCD, the reactor chamber pressure was set at 250 mbar and H_2 and CH_4 flows were kept at 190 sccm and 10 sccm respectively. Meanwhile, the microwave power was set to be at 3500 W. No intentional doping was made during the growth. The sample looks colorless and transparent. The SCD was then cut along the crystal orientation or cleavage plane [400] and the sample size is $8\times8\times1$ mm^3.

The SCD samples were characterized by following methods at room temperature: i) X-ray diffraction (XRD, Empyrean) was applied to examine the crystal structure; ii) Raman spectroscopy was used to measure the characteristic Raman shift, where the excitation wavelengths of 532 nm (InVia, Renishaw plc) and 785 nm (Avaspec, The Netherlands) were used; iii) Fourier transform infrared (FTIR, Nicolet iS 50) spectroscopy was employed to check the C-based bonds; and iv) X-ray photoelectron spectroscopy (XPS, Escalab Xi+, China) was used to evaluate the concentrations of the major elements and the major functional groups attached to the surface of SCD.

3. THz TDS measurement

In the present study, we apply the standard THz TDS technique for the transmission measurement of the SCD [23]. The experimental setup of our THz TDS system is shown schematically in Fig. 1: i) the fs laser beam, generated from a Ti:sapphire regenerative amplifier laser (Coherent Inc., USA. 35 fs pulse width, 800 nm central wavelength, 1 kHz repetition rate, and about 1 mJ output power), is divided into two beams as the pump and probe light sources respectively after passing through a beam splitter; ii) the

pump beam with relatively large intensity is focused on ZnTe crystal to generate the pulsed THz wave with an effective frequency range 0.2-1.2 THz. The THz radiation generated by the ZnTe crystal is linearly polarized; iii) the generated THz beam is focused perpendicularly on the surface of the SCD sample; iv) through a time-delay stage, the probe beam is co-linearly incident to another ZnTe crystal along with the pump beam, which drives the THz detector via the electro-optical (EO) sampling using quarter-wave plate and Wallaston Prism [18]; v) the strength of the THz electric field transmitted through the SCD sample and detected by the EO sampling system is recorded by a lock-in amplifier; and vi) the SCD sample is placed on the sample holder in a superconducting refrigerator (Oxford, UK) with a quartz window, and the sample chamber is in vacuum. Thus, we can measure the strength of the THz electric field transmitted through the SCD as a function of the delay time in the temperature range of 1.5 to 300 K. Additionally, the key part of the THz TDS system is sealed and filled with nitrogen gas (N_2, 4 %) to prevent frost forming on the optical window of the thermostat and the absorption of water vapor to the THz wave. As a result, the signal-to-noise ratio of the measurement can be largely improved [24-25]. The experimental setup in this study is similar to that in our previous studying of the THz optoelectronic properties of carbon nanodots [23].

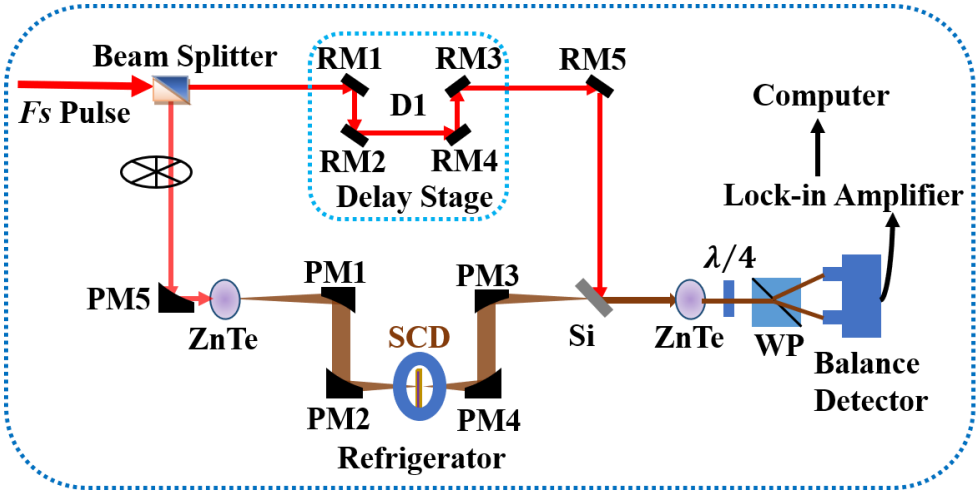

Fig. 1. Schematic diagram of the THz TDS system for transmission measurement. Here, WP, RM, and PM stand respectively for the wollaston prism, reflection mirror, and parabolic mirror. Si is used as THz semi-transparent and semi-reflective mirror and two ZnTe crystals are used for THz generation and detection, respectively.

In the measurement, the incident THz beam is applied perpendicularly to the surface (i.e., the [400] plane) of the SCD and the THz electric field is set to be polarized linearly along the x-direction of the [400] plane of the SCD, which makes the results related to the optoelectronic response along the x-direction in [400] plane of the SCD.

4. Results and discussions

4.1 Structure characterization of the SCD

The XRD spectrum for the SCD sample is shown in Fig. 2(a). There is a sharp peak at 2θ=120°, which corresponds to the [400] crystal face. This indicates that the crystal orientation of SCD originates from the [100] direction and the sample has high crystalline quality. The Raman spectra are shown in Fig. 2(b). The sharp characteristic Raman peaks for SCD can be observed at 1332.5 cm^{-1} with 532 nm excitation and at 1334.42 cm^{-1} with 785 nm excitation. This peak is induced by the G-band Raman shift due to electron interaction with longitudinal optic (LO) phonons in SCD [26]. There is no characteristic peaks of non-diamond carbon phases observed in the spectra, suggesting the excellent quality and purity of the SCD sample. The FTIR spectrum for SCD is shown in Fig. 2(c). It should be noted that the region from 2680 to 1600 cm^{-1} refers to intrinsic multi-phonon absorption from the C-C bonds of the SCD due to dipole momentum changes [16]. The typical diamond peak at 2158 cm^{-1} can be seen clearly.

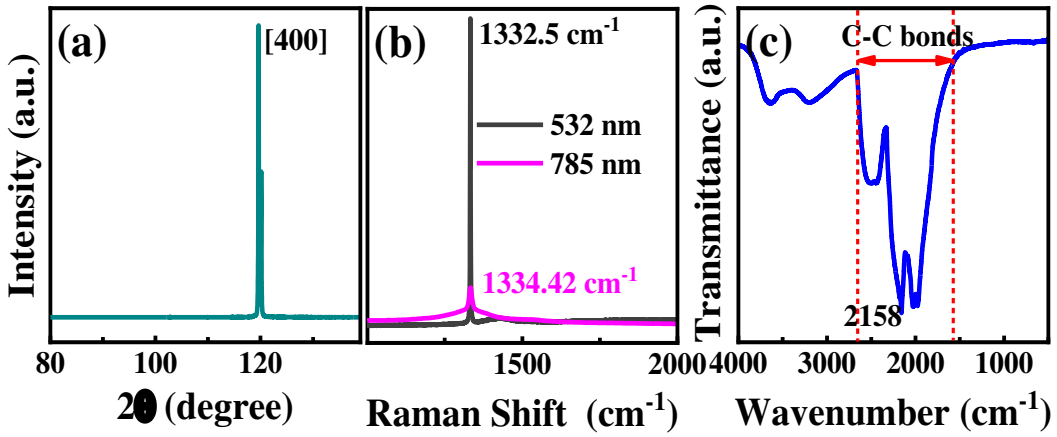

Fig. 2. (a) XRD spectrum, (b) Raman spectra excited by two wavelengths as indicated, and (c) FTIR spectrum of SCD.

Fig. 3(a) shows the full-scan XPS spectrum of the SCD. From the peaks at 284.8 eV, 399.19 eV and 532.07 eV, we learn that the SCD used in this study consist mainly of C (91.72%), O (4.69%) and N (3.57%). The high resolution XPS spectra for C 1s, N 1s and O 1s are shown in Fig. 3(b), (c) and (d), respectively. We note that: i) from Fig. 3(b), the high-resolution C 1s spectrum can be deconvoluted into three contributions from C=C (red curve), C-C (blue curve) and C=O (green curve) bonds, which are peaked at 284.46 eV, 285.01 eV and 287.45 eV, respectively; ii) the N 1s spectrum in Fig. 3(c) can be deconvoluted into two contributions peaked at 399.2 eV for pyridinic N (red curve) and at 399.65 eV for amino N (blue curve); and iii) the O 1s spectrum in Fig. 3 (d) is attributed mainly from -OH (red curve and peaked at 530.95 eV) and C=O (blue curve and peaked at 532.21 eV) based functional groups. It should be particularly noted that the SCD sample was grown by MPCVD with H_2 and CH_4 as feed gases, which can lead to the appearance of hydrogen terminations on the SCD surface [6, 27]. In contrast, conventional XPS cannot measure easily the H-bonding condition on the sample surface because the binding energies of C-H bonds are close to that of C=C bonds. These results indicate that the sample contains small amounts of H-terminations, -OH-, O- and N-based functional groups on the surface of SCD.

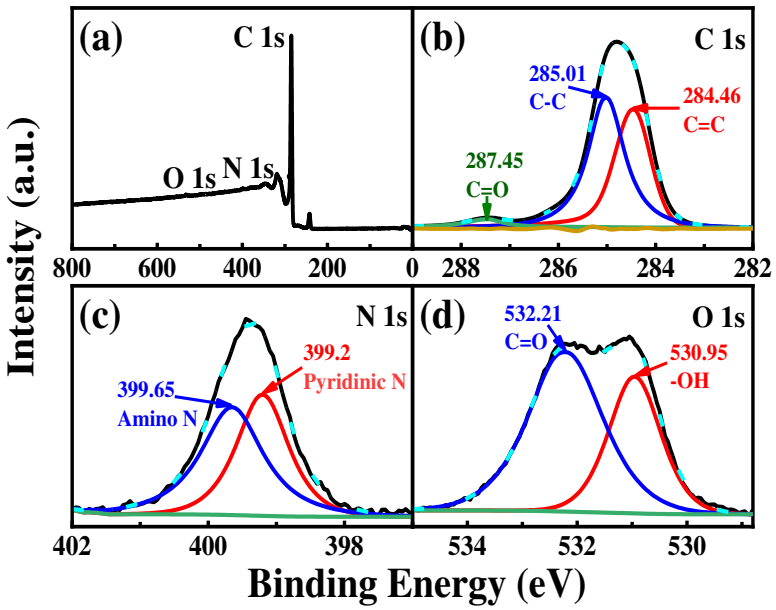

Fig.3. (a) Full-scan XPS spectrum of SCD and the high resolution XPS spectra for C 1s (b), N 1s (c) and O 1s (d), where the contributions from different chemical bonds are indicated.

4.2 THz transmission spectrum

The basic principle of THz TDS is to use fs laser pulse to generate and detect the time-resolved THz electric field transmitted through the sample and to obtain spectral information of the measured sample through Fourier transformation. In recent years, we have applied the THz TDS technique for the investigation of low-dimensional and nanostructured electronic systems such as graphene [28], monolayer (ML) MoS_2 [24, 29], ML WS_2 [30], ML hBN [25, 31], carbon nanodots [23], etc. In the present study, we take a similar approach for studying the optoelectronic properties of SCD. Firstly, we measure the no-load transmission signals in the time-domain at room temperature as reference $E_{ref}(t)$. Then we measure the THz transmission electric field through the SCD sample $E_{scd}(t)$ in the time-domain (see inset in Fig. 4) at different temperatures. The corresponding THz electric fields in the frequency-domain, $E_{scd}(\omega)$ and $E_{ref}(\omega)$, can be obtained via the Fourier transformation of $E_{scd}(t)$ and $E_{ref}(t)$. Fig. 4 shows the amplitude and the phase angle of $E_{scd}(\omega)$ for SCD in the frequency-domain at different temperatures. As we can see, the amplitude of $E_{scd}(\omega)$ decreases and shows a slight blue shift with increasing temperature, whereas the phase angle of $E_{scd}(\omega)$ depends weakly on temperature.

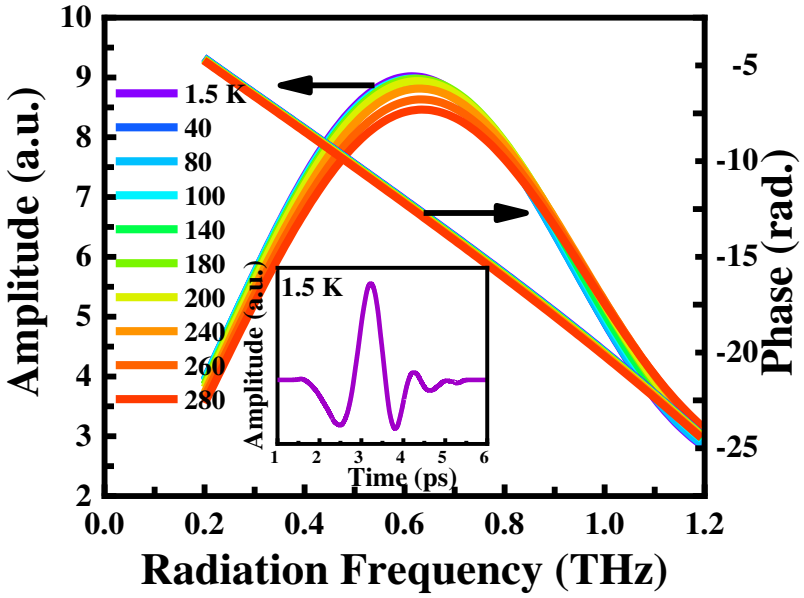

Fig. 4. Amplitude and phase angle of THz electric field as a function of radiation frequency $f=\omega/2\pi$ for SCD at different temperatures as indicated. The inset shows the THz electric field transmitted through the SCD in the time-domain at a fixed temperature of 1.5 K.

From the results of $E_{scd}(\omega)$ and $E_{ref}(\omega)$, we can obtain the THz transmittance of the SCD sample via:

$$T(\omega) \approx \left|E_{scd}(\omega)\right|^2 \Big/ \left|E_{ref}(\omega)\right|^2, \quad (1)$$

where $|E(\omega)|$ is the amplitude of the corresponding THz field in frequency-domain. In Fig. 5, we present the transmittance of SCD as a function of radiation frequency $f=\omega/2\pi$ from 0.2 THz to 1.2 THz for temperatures from 1.5 K to 300 K. In the 0.2-0.7 THz regime, the transmittance decreases with increasing temperature especially in the low-frequency regime, while in 0.7-1.2 THz regime, $T(\omega)$ increases slightly with temperature. Notice that although temperature can affect the transmittance of SCD especially in the low-frequency regime, the room temperature transmittance of SCD is still above 65 % at 0.2 THz and increases markedly with radiation frequency, which is above 80 % for f> 0.65 THz. These results indicate and confirm further that SCD can be used as THz optical window material working in a wide temperature range [3].

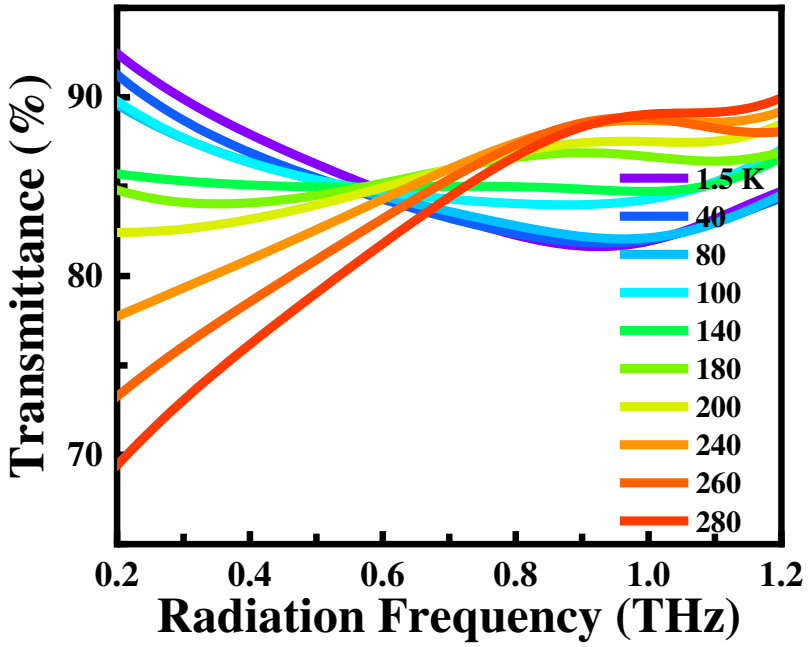

Fig. 5. THz transmission spectrum for SCD as a function of radiation frequency $f=\omega/2\pi$ at different temperatures as indicated.

4.3 Complex optical conductivity and dielectric constant

With $E_{scd}(\omega)$ and $E_{ref}(\omega)$ obtained from THz TDS measurement, we can attain the

complex optical conductivity $\sigma(\omega)=\sigma_1(\omega)+ i\sigma_2(\omega)$ for SCD via the Tinkham formula [23]

$$\frac{E_{scd}(\omega)}{E_{ref}(\omega)}=\frac{1+n}{1+n+Z_0 d\sigma(\omega)}\ , \quad (2)$$

where n=1 is the refractive index of air, d=1 mm is the thickness of SCD sample, and Z_0=377 Ω is the impedance of the free space. The real $\sigma_1(\omega)$ (black circles) and imaginary $\sigma_2(\omega)$ (red circles) parts of the optical conductivity for SCD are shown in Fig. 6. We find that $\sigma_1(\omega)$ and $\sigma_2(\omega)$ for SCD increase slowly with increasing radiation frequency f and temperature. The found behavior of $\sigma_1(\omega)$ and $\sigma_2(\omega)$ do not obey the conventional Drude formula for optical conductivity in an electron gas system [32]. The Drude formula is given as: $\sigma(\omega)=\sigma_0/(1-i\omega\tau)$, where $\sigma_0=n_e e^2\tau/m^*$ is the dc conductivity, n_e is the electron density, τ is the electronic relaxation time, and m^* is the effective electron mass. It suggests that $\sigma_1(\omega)$ should decreases monotonously with increasing ω and $\sigma_1(\omega)$ should show a peak-like shape in the spectrum. In this study, we employ the modified Drude-Smith formula (DSF) [33] for the understanding of the experimental results. By taking only the first collision term in the general Drude-Smith formula into consideration, the DSF can be written as:

$$\sigma(\omega)=\frac{\sigma_0}{1-i\omega\tau}\left[1+\frac{c}{1-i\omega\tau}\right], \quad (3)$$

where the coefficient $c\in$[-1,0] refers to the fraction of original velocity for an electron after a collision event, which corresponds to the effect of photon-induced electronic backscattering or localization [33]. When c=-1, the carriers in the electronic system are fully backscattered or localized. When c=0, the DSF turns to the conventional Drude formula and the carriers are in free motion [33-34]. We find that both $\sigma_1(\omega)$ and $\sigma_2(\omega)$ given by the DSF can fit very well to our experimental results, as shown in Fig. 6 (see solid curves) for temperature from 5 K to 300 K.

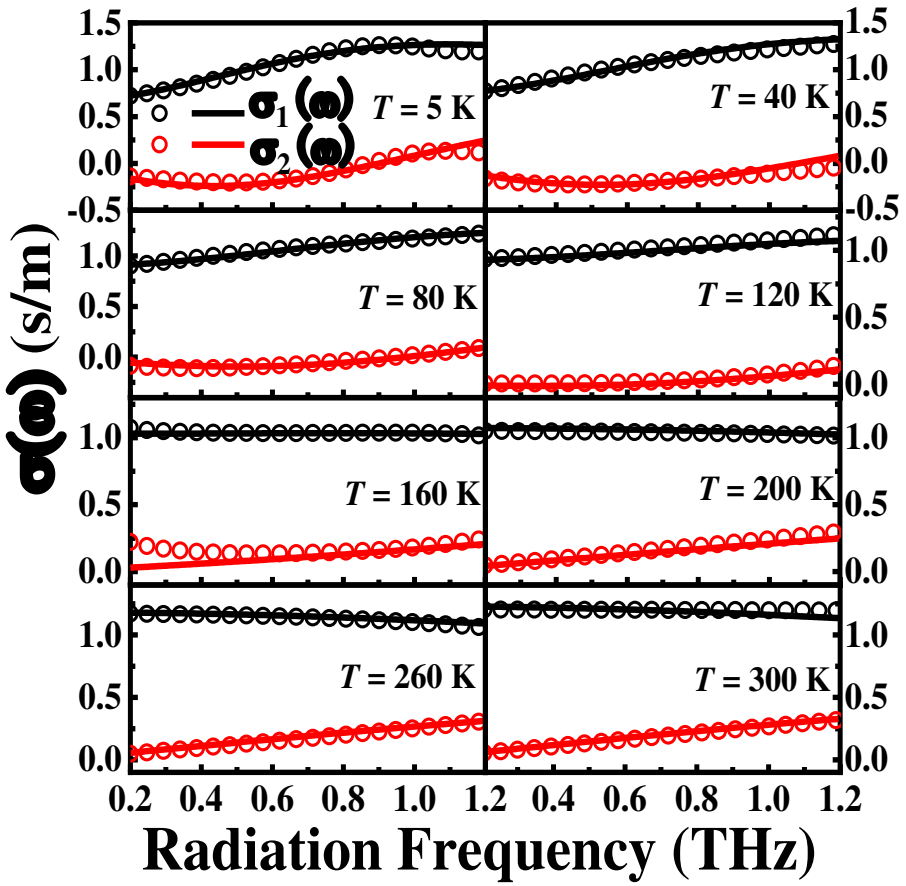

Fig. 6. Real [$\sigma_1(\omega)$, black circle and curve] and imaginary [$\sigma_2(\omega)$, red circle and curve] parts of optical conductivity for SCD as a function of radiation frequency $f=\omega/2\pi$ at different temperatures as indicated. Here the experimental and theoretical results are represented, respectively, by circles and curves.

It is known that in good metals and semiconductors, the optical conductivity induced by free carrier absorption can be described by the Drude formula. However, in poor metals [35] and semiconductors [36] deviations of the optical conductivity from the Drude behavior are observed experimentally. The DSF was proposed to understand the non Drude-like optical conductivity on the basis of electronic backscattering with the help of Poisson statistics [33]. In recent years, the Drude-Smith like optical conductivity has been observed experimentally in nanostructured materials [25], two-dimensional electronic systems [25, 37], carbon nanodots [23], etc. The results shown in Fig. 6 implies that SCD does not show typical features of semiconductor in THz regime. This is because the conducting carriers in SCD come mainly from surface H-terminations, -

OH-, O- and N-based bonds and functional groups in a sample without intentional doping during the sample growth.

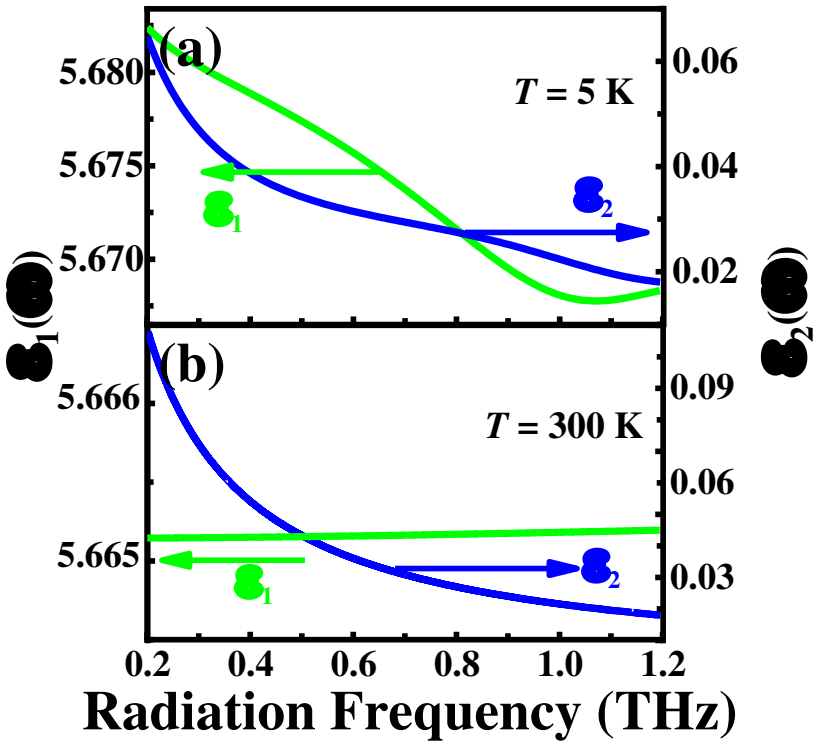

Fig. 7. Real [$\varepsilon_1(\omega)$, green curve] and imaginary [$\varepsilon_2(\omega)$, blue curve] parts of complex dielectric constant for SCD as a function of radiation frequency $f=\omega/2\pi$ at 5 K and 300 K as indicated.

Optical conductivity is one of the most important physical quantities, from which we can obtain optical coefficients such as the absorbance, refractive index, dielectric constant, etc. [25] It is also a bridge quantity between optics and condensed matter physics. For example, the relationship between $\sigma(\omega)$ and the complex dielectric constant for an electronic material is [25]

$$\sigma(\omega)=\sigma_1(\omega)+i\sigma_2(\omega)=-i\omega\varepsilon_0\left[\varepsilon(\omega)-\varepsilon_\infty\right], \quad (4)$$

where $\varepsilon(\omega)= \varepsilon_1(\omega)+ i\varepsilon_2(\omega)$ is the complex dielectric constant, $\omega=2\pi f$ is the angular frequency, ε_0 is the permittivity of the vacuum, and ε_∞ is the permittivity at high frequency. With our experimental data from THz TDS transmission measurement, we can obtain the complex dielectric constants of SCD using Eq. (4), which are shown in Fig. 7 at T=5 K and 300 K. As we can see, $\varepsilon_1(\omega)$ does not vary significantly in 0.2-1.2 THz regime, whereas $\varepsilon_2(\omega)$ depends rather strongly on THz radiation frequency. We

note that the value of $\varepsilon_1(\omega)$ measured here is very close to the static dielectric constant of 5.67 [38-39] at room temperature. Moreover, $\varepsilon_1(\omega)$ and $\varepsilon_2(\omega)$ depend weakly on temperature.

4.4 Key electronic parameters of SCD

From the conditions of sample growth and the XPS results shown in Fig. 3, we know that the major bonds and functional groups attached to the surface of SCD are H-terminations, -OH and C-O based bonds along with pyridinic N and amino N based bonds. They can play the roles like impurities and defects akin to a semiconductor. Moreover, these bonds and defects have electronegativity [40] and, therefore, our SCD sample is n-type and the conducting carriers in SCD are electrons. The effective electron mass for an electron along the x-direction in [100] plane of diamond is m^*=0.23 m_e [41], with m_e being the rest electron mass. Using this value, we are able to fit the experimental results with the DSF. Through fitting $\sigma_1(\omega)$ and $\sigma_2(\omega)$ with the DSF, we can determine the key electronic parameters of the SCD, such as the electron density n_e, the electronic relaxation time τ, and the electronic backscattering or localization factor c.

In Fig. 8(a), the electron density n_e is shown as a function of temperature T. We find that when T is less than 10 K, n_e depends weakly on temperature. When T is larger than 10 K n_e increases with T and can be fitted nicely by the Arrhenius relation:

$$n_e = \alpha \cdot \exp(-\Delta E / k_B T), \quad (5)$$

where $\alpha=2.6\times10^{14}\ cm^{-3}$ and the activation energy is $\Delta E=0.63\ meV$. It implies that the electrons in SCD are in metallic-like phase when $T\leq$10 K and are in semiconductor-like phase when $T>$10 K. The metallic to semiconductor transition temperature is at about 10 K for SCD. Because no intentional doping was made during the sample growth, the SCD used in this study has relatively low electron density. When $T>$10 K, the activation energy for SCD is $\Delta E=0.63\ meV$, indicating that the thermal activation of H-terminations, O- and N-based bonds and functional groups can be easily achieved in SCD and the electron density increases exponentially with temperature from 10 K up

to at least room temperature. Because H- and O-based bonds are very sensitive to THz radiation field [42-43], the thermal activation of electrons can occur more strongly in SCD in the presence of THz radiation.

In Fig. 8(b), the temperature dependence of the electronic relaxation time τ is presented for SCD (red dots). We find that τ decreases with increasing T and can be well fitted by [44]:

$$\frac{1}{\tau} = \frac{1}{\tau_{IM}} + \alpha_{AC} T + \Gamma_{LO} N_0, \quad (6)$$

where τ_{IM} comes from impurity scattering and is independent of T, $1/\tau_{AC}=\alpha_{AC}T$ is attributed to acoustic-phonon scattering with α_{AC} being a fitting parameter, and $1/\tau_{LO}=\Gamma_{LO}N_0$ is the contribution from LO phonon scattering with Γ_{LO} being a fitting parameter, $N_0=[exp(E_{LO}/k_BT)-1]^{-1}$ the LO phonon occupation number, and E_{LO} the LO-phonon energy. For SCD, E_{LO}=165.18 *meV* [45] as is also apparent from in the G-band Raman shift of SCD (see Fig. 2(b)). Through fitting, we obtain τ_{IM}=142.86 *fs,* $\alpha_{AC}=7.143\times10^{10}$ $s^{-1}K^{-1}$ and $\Gamma_{LO}=1.242\times10^{15}$ s^{-1} for SCD. The contributions from different electronic scattering centers in SCD are shown in Fig. 8(b) as a function of temperature (curves). As we can see, the decrease in τ with increasing temperature is mainly caused by electron coupling with acoustic-phonons. This is because the impurity scattering in carbon-based materials depends very little on temperature [46] and the LO-phonon energy in diamond is very large. As a result, the temperature dependence of the electronic relaxation time in SCD is mainly determined by acoustic-phonon scattering up to room temperature [47].

In Fig. 8(c), we show the electronic localization factor c as a function of temperature. We find that the value of c decreases slowly with increasing temperature up to 60 K and it decreases sharply with increasing T in the temperature range from 60 K to 300 K, noting that c is a negative factor. This implies that the photon-induced electronic backscattering or localization weakens with increasing temperature in SCD. When $\omega\rightarrow0$ in Eq. (3), we get: $\sigma(0)=\sigma_0(1+c)$. Thus, the effective electron density in the presence of electronic backscattering in SCD can be obtained as: $n^*=n_e(1+c)$. The temperature dependence of n^* is shown in the inset of Fig. 8(c). Similar to n_e, n^*

depends weakly on T when $T \leq 10$ K and increases with T when $T > 10$ K, indicating that the metallic to semiconductor transition can also be observed by looking at the temperature dependence of the effective electron density in SCD. Because c is a negative factor, n^* is generally less than n_e, implying the electronic localization.

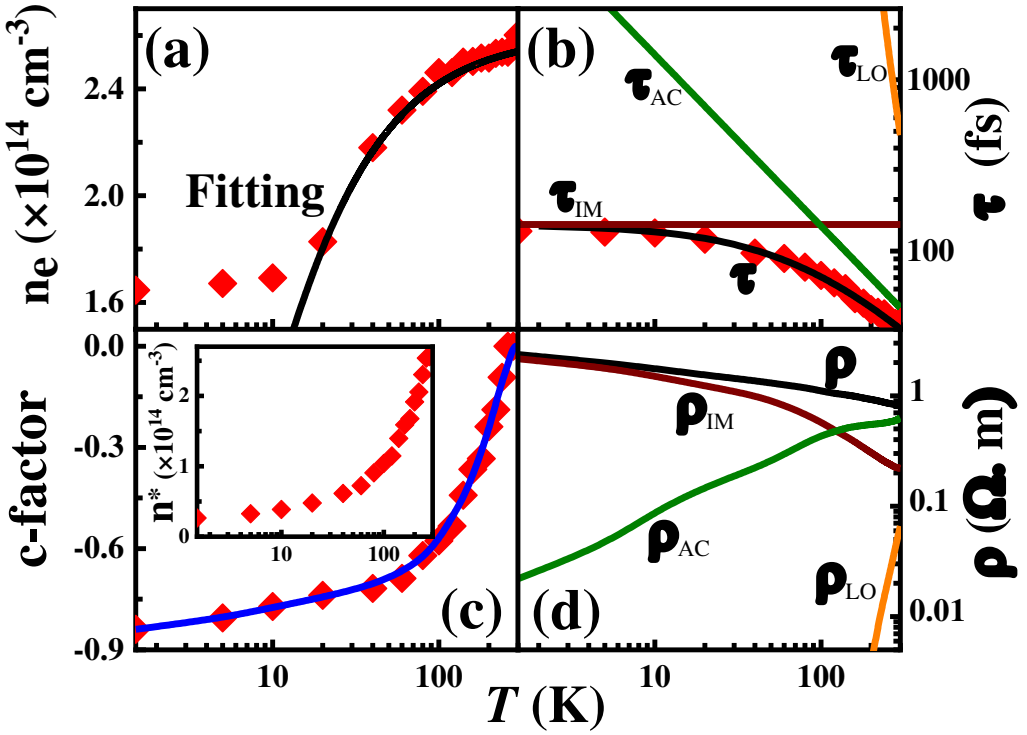

Fig. 8. (a) Electron density n_e, (b) electronic relaxation time τ, (c) electronic localization factor c, and (d) dc resistivity ρ as a function of temperature for SCD. In (a)-(c), the red dots are experimental results, the black curve in (a) is obtained by fitting with Eq. (5), the curves in (b) are obtained by fitting with Eq. (5) and the contributions from different scattering mechanisms are indicated, the blue curve in (c) is drawn to guide the eye, and the inset in (c) shows the temperature dependence of the effective electron density n^* for SCD. In (d), the contributions from different scattering centers to dc resistivity of SCD are presented by using Eq. (6).

By using the sample parameters obtained through fitting the experimental data with the theoretical formula, the dc resistivity $\rho = m^*/(n^* e^2 \tau)$ can be obtained for SCD in the presence of photon-induced electronic backscattering or localization effect. In Fig. 8(d), the contributions to ρ from different electronic scattering mechanisms, ρ_{IM}, ρ_{AC} and ρ_{LO}, are plotted as a function of temperature. We note that ρ depends weakly on

temperature when $T \leq 60$ K and decreases rather slowly with increasing temperature when $T > 60$ K due to electron coupling with acoustic-phonons [3]. The temperature dependence of ρ for SCD looks weaker than that of n_e and of τ (see Fig. 8(a) and (b)), because the decrease in τ is partial offset by the increase in n_e with increasing temperature. Furthermore, from dc resistivity obtained from THz TDS measurement, we can estimate the square resistance of our SCD sample, which is about 10^3 Ω at room temperature. The values of the electron density and the square resistance for SCD, measured via THz TDS in this work, are in line with those obtained from electric transport measurements [27].

4.5 Further remarks

It has been shown that H- and O-based bonds and functional groups are very sensitive to THz radiation fields [43, 48]. From the conditions of our sample growth and the XPS results shown in Fig. 3, we learn that the major bonds and functional groups attached to the surface of SCD are H-terminations, -OH and C-O based. The THz radiation can affect strongly the vibration and rotation of these bonds and functional groups which are with electronegativity [40]. Therefore, the strong optoelectronic response to THz radiation can be observed experimentally in SCD.

One of the most interesting and important findings from this work is that there is a metallic to semiconductor transition in SCD at about 10 K, observed via examining the temperature dependence of the electron density (see Fig. 8(a)). Because the conducting electrons in SCD come mainly from H-terminations, -OH-, O- and N-based bonds and functional groups attached to the surface of SCD, these defects and impurities cannot be thermally activated at low temperatures. Thus, the electron density in SCD in low temperature regime does not alter with temperature and shows a metallic behavior when $T \leq 10$ K. In relatively high temperature regime, the thermal activation of surface H-terminations, -OH-, O- and N-based bonds and functional groups in SCD becomes possible and, thus, the temperature dependences of the electron density and the dc resistivity in SCD show the typical behaviors of a semiconductor. It should be noted that in SCD at relatively high temperatures, with increasing temperature the increase in

electron density is quicker than the decrease in electronic relaxation time due to phonon scattering. Hence, the dc resistivity decreases with increasing temperature. Our results shown in Fig. 8(d) is in consistent with those obtained from transport measurement on SCD [1].

5. Conclusions

In this study, we have prepared high quality synthetic single crystalline diamonds (SCDs) by using the MPCVD technique. The THz TDS has been applied to measure the optical coefficients of SCD, such as the transmittance, the complex dielectric constant and the complex optical conductivity. Through fitting the experimental results with theoretical formula, we have obtained optically the key electronic parameters of SCD. The temperature dependence of these sample parameters has been examined. The main conclusions drawn from this study can be summarized as follows.

We have found that there are the H-terminations, -OH-, O- and N-based bonds and functional groups in the surface of SCD grown by MPCVD technique. These bonds and functional groups are the major sources of conducting electrons in SCD without intentional doping during the sample growth. This is the main difference between SCD and natural diamond in which more impurities and detects can be presented.

The transmittance of SCD depends on temperature and THz radiation frequency. However, it is above 65% at room temperature in 0.2-1.2 THz and increases with increasing radiation frequency and decreasing temperature. This finding confirms that SCD is a good material for THz optical window.

The real and imaginary parts of dielectric constant of SCD depend weakly on temperature. $\varepsilon_1(\omega)$ does not vary significantly in 0.2-1.2 THz regime and is close to the static dielectric constant of SCD. However, $\varepsilon_2(\omega)$ depends rather strongly on THz radiation frequency.

It is suggested that SCD is not a good semiconductor in THz regime. Its optical conductivity cannot be described rightly by the conventional Drude formula. However, the modified Drude-Smith formula for optical conductivity can be employed to fit nicely the experimental results. Through fitting, we have determined optically the key

electronic parameters of SCD, such as the electron density, the electronic relaxation time and the electronic localization factor.

We have found that there is a metallic to semiconductor transition at about T=10 K and the temperature dependence of electronic relaxation time is mainly induced by electron coupling with acoustic-phonons. Moreover, there is a significant effect of photon-induced electronic backscattering or localization in SCD.

In this study, we have demonstrated that THz TDS is a powerful optical tool in the investigation of SCD with high dc resistivity and low electron density and in the presence of H- and O-based bonds and functional groups. By using this advanced technique, we can measure directly and more accurately not only the complex optical coefficients but also the key material parameters of SCD. More particularly, the determination of the electron density in SCD can be achieved without the need of making contact electrodes and of applying an external magnetic field. We hope that the interesting and important findings obtained and observed in this study can help us to gain more understanding of SCD and can provide a research basis for the application of SCD as electronic, optical and optoelectronic material.

Acknowledgements

This work was supported by the National Natural Science foundation of China (NSFC) (Grants No. U1930116, No. U206720039, No. 12004331), Shenzhen Science and Technology Program (No. KQTD20190929173954826), the University Engineering Research Center of Crystal Growth and Applications of Guangdong Province (2020GCZX005), Special Innovative Projects of Guangdong Province (2020KTSCX125), and Shenzhen Stable Supporting Program (SZWD2021015).

References

[1] D. Das and M.S. Ramachandra Rao, N^+-ion implantation induced enhanced conductivity in polycrystalline and single crystal diamond, RSC Adv. 11 (2021) 23686.

[2] S.K. Tiwari, R. Pandey, N.N. Wang, V. Kumar, O.J. Sunday, M. Bystrzejewski, et al., Progress in Diamanes and Diamanoids Nanosystems for Emerging Technologies, Adv. Sci. 9 (2022)

2105770.

[3] A.H. Piracha, K. Ganesan, D.W.M. Lau, A. Stacey, L.P. McGuinness, S. Tomljenovic-Hanic, et al., Scalable fabrication of high-quality, ultra-thin single crystal diamond membrane windows, Nanoscale 8 (2016) 6860.

[4] P. Siyushev, M. Nesladek, E. Bourgeois, M. Gulka, J. Hruby, T. Yamamoto, et al., Photoelectrical imaging and coherent spin-state readout of single nitrogen-vacancycenters in diamond, Science 363 (2019) 728–731.

[5] E. Bourgeois, A. Jarmola, P. Siyushev, M. Gulka, J. Hruby, F. Jelezko, et al., Photoelectric detection of electron spin resonance of nitrogen-vacancy centres in diamond, Nat. Commun. 6 (2015) 8577.

[6] D. Shin, B. Rezek, N. Tokuda, D. Takeuchi, H. Watanabe, T. Nakamura, et al., Photo- and electrochemical bonding of DNA to single crystalline CVD diamon, Phys. Stat. Sol. (a) 203 (2006) 3245–3272.

[7] Y. Gao, N. Gao, H.D. Li, X.X. Yuan, Q.L. Wang, S.H. Cheng, et al., Semiconductor SERS of Diamond, Nanoscale 10 (2008) 15788-15792.

[8] M. Kobayashi, S. Yoshihashi, K. Ogawa, M. Isobe, S. Sangaroon, S. Kamio, et al., A comprehensive evaluation of the thermal neutron detection efficiency by a single crystal CVD diamond detector with a LiF thermal neutron converter, Fusion Eng. Des. 179 (2022) 113117.

[9] A.H. Piracha, P. Rath, K. Ganesan, S. Kuehn, W. HP Pernice, and S. Prawer, Scalable Fabrication of Integrated Nanophotonic Circuits on Arrays of Thin Single Crystal Diamond Membrane Windows, Nano. Lett. 16 (2016) 3341–3347.

[10] W. Deferme, A. Bogdan, G. Bogdan, K. Haenen, W. De Ceuninck, and M. Nesládek, Electrical transport measurements and emission properties of freestanding single crystalline CVD diamond samples, Phys. Stat. Sol. (a) 204 (2007) 3017–3022.

[11] G.F. Zhang, T. Samuely, J. Kačmarčík, E.A. Ekimov, J. Li, V.V. Moshchalkov, et al., Bosonic Anomalies in Boron-Doped Polycrystalline Diamond, Phys. Rev. Appl. 6 (2016) 064011.

[12] N. Cennamo, P.A.S. Jorge, Optical Measurements, IEEE Instru. Meas. Mag. 24(5) (2021) 3-4.

[13] Y. Zhang, Y.N. Chen, Y.L. Liu, F.B. Fu, W.C. Yu, P. Jin, et al., Research on band-edge emission properties and mechanism of high-quality single-crystal diamond, Carbon 132 (2018) 651-655.

[14] S.A. Malykhin, R.R. Ismagilov, F.T. Tuyakova, E.A. Obraztsova, P.V. Fedotov, A. Ermakova, et al., Photoluminescent properties of single crystal diamond microneedles, Opt. Mater. 75 (2018) 49-55.

[15] A.P. Bolshakov, V.G. Ralchenko, G.Y. Shu, B. Dai, V.Y. Yurov, E.V. Bushuev, et al., Single crystal diamond growth by MPCVD at subatmospheric pressures, Mater. Today Commun. 25 (2020) 101635.

[16] Y.F. Wang, W.F. Zhang, C.N. Lin, P.P. Ren, Y.J. Lu, C.X. Shan, et al., Multiphoton Upconversion Emission from Diamond Single Crystals, ACS Appl. Mater. Inter. 10 (2018) 18935−18941.

[17] T.P. Mollart, K.L. Lewis, C.S.J. Pickles, and C.J.H. Wort, Factors affecting the optical performance of CVD diamond infrared optics, Semicond. Sci. Tech. 18 (2003) S117–S124.

[18] A. Rubano, S. Mou, L. Marrucci, and D. Paparo, Terahertz Hyper-Raman Time-Domain Spectroscopy, ACS Photonics 6 (2019) 1515−1523.

[19] S. Amoruso, A. Andreone, A. Bellucci, C. Koral, M. Girolami, M. Mastellone, et al., All-carbon THz components based on laser-treated diamond, Carbon 163 (2020) 197-201.

[20] Y.T. Zheng, R. Zhang, X.D. Chen, P. Hing, J.L. Liu, J.J. Wei, et al., Doomed Couple of Diamond with Terahertz Frequency: Hyperfine uality Discrimination and Complex Dielectric Responses of Diamond in the Terahertz Waveband, ACS Appl. Electron. Mater. 2 (2020) 1459−1469.

[21] B.C. Lin, Q. Song, D.Q. Pang, B.W. Liu, W.P. Kong, Z.Y. Li, et al., Optical grating and THz polarizer based on normal grade single crystal diamond fast fabricated by fs laser, Infrared Phys. Techn. 115 (2021) 103703.

[22] K.W. Hemawan, H.Y. Gou and R.J. Hemley, Diamond synthesis at atmospheric pressure by microwave capillary plasma chemical vapor deposition, Appl. Phys. Lett. 107 (2015) 181901.

[23] D. Song, J.K. Tian, W. Xu, H. Wen, C. Wang, J. Tang, et al., Optically induced insulator-to-semiconductor transition in fluorescent carbon quantum dots measured by terahertz time-domain spectroscopy, Carbon 174 (2021) 741-749.

[24] C. Wang, W. Xu, H.Y. Mei, H. Qin, X.N. Zhao, C. Zhang, et al., Substrate-induced electronic localization in monolayer MoS_2 measured via terahertz spectroscopy, Opt. Lett. 44 (2019) 4139–4142.

[25] M. Bilal, W. Xu, C. Wang, H. Wen, X.N. Zhao, D. Song, et al., Optoelectronic Properties of Monolayer Hexagonal Boron Nitride on Different Substrates Measured by Terahertz Time-Domain Spectroscopy, Nanomaterials 10 (2020) 762.

[26] S. Prawer and R.J. Nemanich, Raman spectroscopy of diamond and doped diamond, Phil. Trans. R. Soc. Lond. A 362 (2004) 2537–2565.

[27] W. Wang, C. Hu, F.N. Li, S.Y. Li, Z.C. Liu, F. Wang, et al., Reprint of "Palladium Ohmic contact on hydrogen-terminated single crystal diamond film", Diam. Relat. Mater. 63 (2016) 175–179.

[28] H.Y. Mei, W. Xu, C. Wang, H.F. Yuan, C. Zhang, L. Ding, et al., Terahertz magneto-optical properties of bi- and tri-layer graphene, J. Phys.: Condens. Matter. 30 (2018) 175701.

[29] H. Wen, W. Xu, C. Wang, D. Song, H.Y. Mei, J. Zhang, et al., Magneto-optical properties of monolayer MoS_2-SiO_2/Si structure measured via terahertz time-domain spectroscopy, Nano. Select. 2 (2021) 90–98.

[30] H.M. Dong, Z.H. Tao, L.L. Li, F. Huang, W. Xu, and F.M. Peeters, Substrate dependent terahertz response of monolayer WS_2, Appl. Phys. Lett. 116 (2020) 203108.

[31] M. Bilal, W. Xu, H. Wen, X.J. Cheng, Y.M. Xiao, and L. Ding, Terahertz optical Hall effect in p-type monolayer hexagonal boron nitride on fused silica substrate, Opt. Lett. 46 (2021) 9.

[32] H. Němec, P. Kužel, and V. Sundström, Far-infrared response of free charge carriers localized in semiconductor nanoparticles, Phys. Rev. B 79 (2009) 115309.

[33] N.V. Smith, Classical generalization of the Drude formula for the optical conductivity, Phys. Rev. B Condens. Matter. 64 (2001) 155106.

[34] T.L. Cocker, D. Baillie, M. Buruma, L.V. Titova, R.D. Sydora, F. Marsiglio, et al., Microscopic origin of the Drude-Smith model, Phys. Rev. B 96 (2017) 205439.

[35] D. Wang, Generalized Drude model and electromagnetic screening in metals and superconductors, Chin. Phys. B 27 (2018) 057401.

[36] C.Y. Tsai, C.Y. Tsai, C.H. Chen, T.L. Sung, T.Y. Wu, and F.P. Shih, Theoretical Model for Intravalley and Intervalley Free-Carrier Absorption in Semiconductor Lasers: Beyond the Classical Drude Model, Ieee J. Quantum Elect. 34 (1998) 3.

[37] K. Wolff, R. Schäfer, M. Meffert, D. Gerthsen, R. Schneider, and D. Fuchs, Anisotropic electronic transport of the two-dimensional electron system in $Al_2O_3/SrTiO_3$ heterostructures, Phys. Rev. B 95 (2017) 245132.

[38] H.T. Ye, C. Q, Sun, H.T. Huang, P. Hing, Single semicircular response of dielectric properties of diamond films, Thin Solid Films 381 (2001) 52-56.

[39] Q.F. Huang, S.F. Yoon, Rusli, Q. Zhang, J. Ahn, Dielectric properties of molybdenum-containing diamond-like carbon films deposited using electron cyclotron resonance chemical vapor deposition, Thin Solid Films 409 (2002) 211–219.

[40] T. Sharda, A.K. Sikder, D.S. Misra, A.T. Collins, S. Bhargava, H.D. Bist, et al., Studies of defects and impurities in diamond thin films, Diam. Relat. Mater. 7 (1998) 250-254.

[41] H. Löfås, A. Grigoriev, J. Isberg, and R. Ahuja, Effective masses and electronic structure of diamond including electron correlation effects in first principles calculations using the GW-approximation, Aip Adv. 1 (2011) 032139.

[42] H. Wang, S. Tsuchikawa, T. Inagaki, Terahertz time-domain spectroscopy as a novel tool for crystallographic analysis in cellulose: the potentiality of being a new standard for evaluating crystallinity, Cellulose 28 (2021) 5293–5304.

[43] M. Takahashi, Terahertz Vibrations and Hydrogen-Bonded Networks in Crystals, Crystals 4 (2014) 74-103.

[44] W. Xu, F.M. Peeters, T.C. Lu, Dependence of resistivity on electron density and temperature in graphene, Phys. Rev. B Condens. Matter. 79 (2009) 48-51.

[45] J. Kulda, H. Kainzmaier, D. Strauch, B. Dorner, M. Lorenzen, and M. Krisch, Overbending of the longitudinal optical phonon branch in diamond as evidenced by inelastic neutron and x-ray scattering, Phys. Rev. B 66 (2002) 241202.

[46] W. Kiciński, S. Dyjak, Transition metal impurities in carbon-based materials: Pitfalls, artifacts and deleterious effects, Carbon 168 (2020) 748-845.

[47] W. Walukiewicz, Acoustic-phonon scattering in modulation-oped heterostructures, Phys. Rev. B 37 (1988) 8530.

[48] Q.C. Liu, Q. Zhang, G.L. Li, Z.C. Guo, X.Y. He, C. Xie, et al., Terahertz spectral investigation of temperature induced polymorphic transformation of 2,2 dinitroethylene-1,1-diamine, RSC Adv. 11 (2021) 6247.